RSC Advances

ROYAL SOCIETY OF CHEMISTRY

www.rsc.org/advances

Journal Name

ARTICLE

Controllable hydrothermal synthesis of Al-doped ZnO with different microstructures, growth mechanisms, and gas sensing properties

LI ZAN[a,b],QIN WEI[c],WU XIAOHONG[a,*]

Received 00th January 20xx,
Accepted 00th January 20xx

DOI: 10.1039/x0xx00000x

www.rsc.org/

Abstract: A series of Al-doped ZnO (AZO) structures, including disk-like, flake-like, flower-like and dumbbell-like morphologies, have been synthesized by a hydrothermal method without any catalyst or template. The morphologies of these AZO structures can be conveniently controlled, by selecting the additives and controlling the experimental conditions, and the result has excellent reproducibility. The gas sensors based on AZO were fabricated and the gas sensing properties were investigated. The sensors showed high response values and reproducible response-recovery for 5-500 ppm ethanol at 332°C, comparing with NH_3, CH_3OH, H_2, CO, HCHO, $NO_x$and a specific mechanism was proposed.

1.Introduction

Volatile organic compounds (VOCs) such as alcohols and aromatic hydrocarbons are potentially hazardous to human health due to their capabilities to stimulate the mucous membranes and upper respiratory tracts[1]. Therefore, it is important to develop a highly responsive and selective sensor for the detection of VOCs.

Recently, AZO (Al-doped ZnO) has been attracted considerable attention due to their excellent electrical performance in gas sensitivity materials[2-4]. When ZnO is doped with Al, it is expected that the dopants act as singly charged donors and supply the excess carriers to conduction band, which will increase the conductivity[5]. Appropriate donor doping can produce the electronic defects that increase the influence of adsorbates on the conductivity. All of these provide a route to improve the sensitivity. AZO material is the new competitive and promising candidate for applications in gas sensors.

S.C. Navale et al.[6] reported selective NO_x sensing characteristics of Al-doped ZnO synthesized in the form of porous pellets sintered at 350°C, and the sensor can detect small concentrations of NO_x at lower operating temperature. P.P. Sahaya et al. [2] studied the gas sensing properties of Al-doped zinc oxide (ZnO) thin films prepared by chemical spray pyrolysis technique. It is observed that Al-doped films show higher sensitivity to methanol vapour comparing with the undoped ZnO film. L.M. et al.[7] reported the synthesis of Al-doped ZnO nanotetrapods by thermal evaporation of the

[a] School of Science, Harbin Institute of Technology, Harbin, 150001, China. E-mail: wuxiaohong@hit.edu.cn; Fax: +86 451 86402522; Tel: +86 451 86402522
[b] School of Science, Harbin University, Harbin,150086,China. E-mail: lizan80@126.com; Fax: +86 451 86402522; Tel: +86 451 86402522
[c] School of Materials Science and Engineering, Harbin Institute of Technology, Harbin, 150001, China. E-mail: qinwei@hit.edu.cn;Fax: +86 451 86402522; Tel: +86 451 86402522

mixed powders of Zn and Al with the weight ratio of 5:1, and the ethanol sensing properties are effectively improved by Al doping. Satish S et al.[4] developed a facile spray pyrolysis route to deposit aluminium doped ZnO (AZO) thin films on to the glass substrates and discussed the gas sensing to H_2S gas. Aluminum doped zinc oxide films were prepared by a sol-gel process using two different precursors by Yue Hou et al.[8] and the gas sensing properties were investigated for different concentrations of hydrogen in the air. However, literature research shows Al-doped ZnO gas sensing material is seldom prepared by hydrothermal synthesis. As we know, the morphology has a significant influence on the gas sensing properties of materials [9-11]. The crystal morphologies can be controlled easily by hydrothermal method.

Atpresent AZO powders can be prepared by solid phase synthesis, gas-phase synthesis, solution synthesis, and some special methods in order to synthesize specific materials such as electrodeposition [12-14]. Hydrothermal synthesis, as an important method of solution synthesis, has been proven to be a versatile approach for preparation of various AZO microstructures due to the narrow size distribution, sufficient crystallization and high-quality growth orientation [15-16].

In this paper, we report the synthesis and characterization of several different microstructures of Al doped ZnO with different exposing crystal planes by adjusting the solvents. The gas-sensing properties of AZO-based sensors to NH_3, CH_3OH, H_2, CO, HCHO, C_2H_5OH and NO_x have been investigated. The hexagonal disk-based sensor with the most exposed (0001) facet show superior sensing property, while the other microstructures demonstrate degenerated performance in the order of disk>flower>dumbbell.

2. Experiments

2.1 Preparation and characterization of materials

All the chemicals are analytical grade reagentsand usedas-received without further purification. The precursor solution was prepared by dissolving $Zn(CH_3COO)_2.2H_2O$ and hexamethylenetetramine(HMT) in 35 ml deionized water with continuous stirring(C_{Zn2+} = 0.1, 0.075, 0.05 and 0.025 mol/L). Make sure that the concentration of HMT is twice the concentration of Zn^{2+}.Subsequently, $Al(NO_3)_3{\cdot}9H_2O$ (Al molar%=3%) was introduced into the above homogeneous solution and magnetically stirred for 10 min. In a typical procedure, this mixture was transferred into a Teflon-lined stainless steel autoclave of 50 ml. Hydrothermal treatments were carried out at 120°C for 12 h, and then the autoclave was cooled down to room temperature naturally. White precipitates were collected by centrifugation, and washed with deionized water and ethanol several times to remove impurities. The precipitates were dried in air at 60°C for 12 h. At last, the final product was obtained through heat treatment at 500°C for 1 h. By comparison, the effect of solvents, such as ethanol and water instead of pure water was investigated separately.

2.2 Characterization

The phase structure and phase purity of the as-synthesized powders were examined by X-ray diffraction (XRD, Japan Dmax-rB X-ray diffractometer with Cu Kα radiation, λ=0.15418nm) at 40 kV, 100 mA over the 2θ range 10-90°. The general morphology of the products was examined by scanning electron microscopy (SEM) on a HITACHI SU8000 instrument operated at 20 kV and equipped with an energy-dispersive X-ray analyzer. The Brunauer-Emmett-Teller (BET) surface area and pore size distribution of the product were obtained from nitrogen physisorption isotherms (adsorption-desorption branches) at 77 K on a Micromeritics Tristar 3000 instrument. Prior to the BET measurement, the sample was degassed overnight under vacuum at 150 °C to vaporize water molecules adsorbed on the material.

2.3 Gas sensor fabrication and test

The fabrication procedure for the heater gas sensors is similar to the method used in previous reports[17].The Al doped ZnO(AZO) powders were mixed with Terpineol, then the paste was formed. The resulting paste was coated on an alumina tube-like substrate on which a pair of Au electrodes had been printed previously, followed by drying at room temperature for about 1 h and subsequent annealing at 600°C for about 2h. Finally, a small Ni-Cr alloy coil was inserted into the tube as a heater, which provided the working temperature of the gas sensor. The schematic drawing of the as-fabricated gas sensor is shown in Figure 1(a).

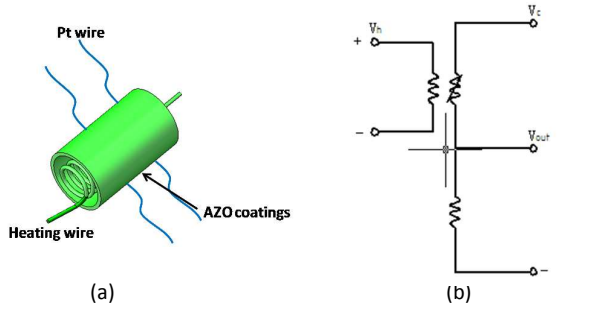

Figure 1.The schematic drawing of the as-fabricated gas sensor(a) and the measurement of electric circuit for gas sensors(b)

In order to improve the long-term stability, the sensors aged at the working temperature for seven days. A stationary state gas distribution method was used for testing gas response (Air humidity: 49.3%). In the measurement of electric circuit for gas sensors (Figure 1b), a load resistor was connected in series with a gas sensor. The gas-sensing properties of the AZO were determined using a HW-30A gas sensitivity instrument (Hanwei Electronics Co. Ltd., PR China). The measurement followed a stationary state gas distribution process, in which a given amount of tested gas was injected into an 18 L glass chamber and fully mixed with air. The gas-sensing test was linked to a mechanical rotary pump capable of evacuating the test chamber down to 5×10^{-2} mbar. Before the sample annealing and each sensing test, the chamber was evacuated and followed by Ar flushing for three times, and then filled with Ar to the atmosphere pressure. Several cycles

of gas sensing test were performed, with each cycle consisting of (1)injecting target gas; (2) retaining target gas pressure within the chamber; and (3) purging the chamber with Ar. Commercially diluted target gas was injected into thetest chamber with a syringe. In the measuring electric circuit as shown in Fig. 1(b), a load resistor (R_L: 47 kΩ) was connected in series with a gas sensor. The circuit voltage (V_c) was 5 V, and output voltage (V_{out}) was the terminal voltage of the load resistor. The working temperature of a sensor was adjusted by varying the heating voltage (V_h). The resistance of a sensor in air or a test gas was measured by monitoring the value of V_{out}.

The system measures the voltages (V_{out}) loaded on the resistor R_L. Therefore, the response value (S) of the gas sensor can be calculated according to the following equations:

$$Ra=[V_c-(V_{out})air\ ]R_L/(V_{out})air \quad (1)$$

$$Rg=[V_c-(V_{out})gas\ ]R_L/(V_{out})gas \quad (2)$$

and

$$S=R_a/R_g. \quad (3)$$

The sensor response is defined as the ratio of the sensor electrical resistance in air (R_a)to that in target gas (R_g). Here, the response time is defined as the time taken for the sensor to achieve 90% of the total response change. The recovery time denotes the time required until 90% of the original baseline signal is recovered.

The gas sensing properties were measured in the working temperatures at 240, 273, 332, and 383°C through adjusting heating voltage to 4, 4.5, 5 and 5.5 V individually. Detecting gases, such as NH_3, CH_3OH, H_2, CO, HCHO, C_2H_5OH and NO_x were injected into a test chamber and mixed with air.

3. Results and discussion

3.1 Composition and Morphology

The XRD patterns of Al doped ZnO and the pure ZnO are shown in Fig. 2(a). All as-obtained powders using a concentration ratio of Zn^{2+} precursor solution to HMT of 1 : 2 show similar XRD patterns. The representative products, prepared with $Zn(CH_3COO)_2{\cdot}2H_2O$ and hexamethylenetetramine(HMT)(C_{Zn2+}:C_{HMT} = 1:2) using different solvents at 120°C, can be indexed to hexagonal wurtzite ZnO with lattice constants of a = 0.325 and c = 0.521 nm (JCPDS card no. 36-1451). Furthermore, the strong and sharp diffraction peaks suggested that the products were highly crystalline. As shown in Table 1, it appeared that the main diffraction peak(101), (100) and (002) of pure ZnO was shifted. The corresponding lattice fringes changed after Al doping. The ionic radius of Al^{3+} is 0.0535 nm, which is smaller than that of Zn^{2+}(0.074 nm)so distortion of lattice will occur only if Al^{3+} replaces Zn^{2+} in ZnO. Besides, the diffraction intensity ratio of the (0001) plane to the $(10\bar{1}0)$ plane (I(0002)/I($10\bar{1}0$)) gradually becomes weaker with the increase in ethanol in Table 2. A higher I(0002)/I($10\bar{1}0$)value means a larger fraction of the (0001) plane, indicating that the exposure of the (0001) plane is dominant. It can be seen that crystallite growth occurs with the increase in ethanol. When the volume ratio of ethanol to water is 20:15, the extracted crystallite size in the $[10\bar{1}0]$ direction is larger in comparison to that in the [0001] direction, implying that the shape of the crystallites is flower-like. When the volume of ethanol was further increased from 20 to 35, the crystallite size in the $[10\bar{1}0]$ direction was smaller than that in the [0001] direction, indicating that the shape of the crystallites is dumbbell-like.

In Fig. 2a, the XRD pattern of the products prepared with V_{C2H5OH}:V_{H2O}=0:35, except for the diffraction peaks of ZnO, small diffraction peaks can be observed clearly.The peaks about at 33°, 40°, 42° and 55° are the diffraction of the(1 2 2), (0 0 4), (2 0 2) and (1 1 5)planes of Al_2O_3.

Table1 XRD data of three sharp peaks in AZO and ZnO

	The position(°)			interplanar spacing (0.1nm)		
	（101）	（100）	（002）	(1 0 1)	(1 0 0)	(0 0 2)
a	36.263	31.764	34.431	2.4752	2.8137	2.6026
b	36.164	31.699	34.444	2.4817	2.8204	2.6016
c	36.243	31.714	34.402	2.4765	2.8191	2.6047
d	36.301	31.809	34.463	2.4727	2.8109	2.6003

Table 2 The diffraction intensity ratio of I(0002)/I($10\bar{1}0$)

V_{C2H5OH}:V_{H2O}	0:35	25:10	35: 0
I(0002)/I($10\bar{1}0$)	0.520	0.436	0.391

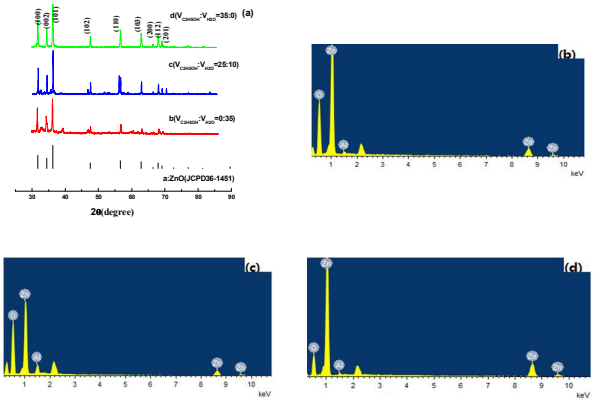

Fig. 2 XRD patterns of as-synthesized AZO powder and pure ZnO(a); EDS pattern of the hexagonal disk(b),dumbbell-like(c) and flower-like(d) AZO

The elemental composition of the as-synthesized AZO was carried out using EDX integrated with SEM instrument as predicted in Fig. 2(b), (c), (d). From EDX measurements, the presence of Zn, O and Al and their compositions are determined. The incorporation of Al in/on ZnO was further demonstrated by the energy diffraction spectrum (EDS) which exhibited the presence of Al element in the bulk of the ZnO besides Zn and O. The percentage calculation of AZO is consistent with the percentage of dopant atom taken during the sample preparation. Thus, EDX measurements confirm that Al dopant is substituted for Zn. In mechanism, the substitution of Al^{3+} ions for Zn^{2+} in ZnO lattice results in one extra electron, thus it produces n-type impurity. However, in order to maintain charge neutrality, the intrinsic defects are produced

simultaneously. For example substitution of two Al^{3+} ions replaces two Zn^{2+} ions and creates one zinc vacancy as a consequence of stoichiometric.

As we know, EDS technique does not provide exact concentration of the elements present in the examined compound. XPS has been measured to establish the exact concentration of the used host/dopant elements. Fig. 3showed the XPS data of AZO for x = 3.18 pp at% Al.

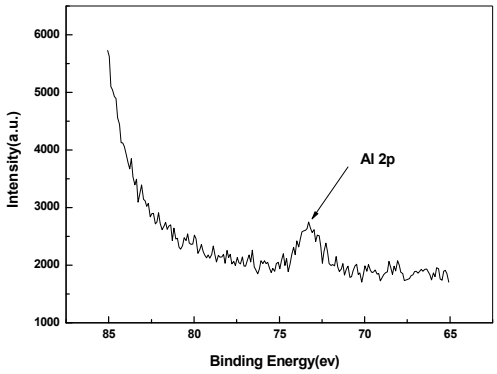

Fig.3 Typical XPS data of Al 2p in AZO for x = 3.18 pp at% Al

3.2 The controllable synthesis of AZO microstructures

Fig.4 manifests the morphologies and the structural characterizations of the as-synthesized products prepared by different concentrations of reactants using deionized water as solvent(C_{Zn2+} = 0.1/0.075/0.05/0.025 mol/L). In Fig.4(a) it can be seen that AZO are microflakes in a large-scale area, which have approximately uniform morphologies. As further shown in the high magnification SEM image (Fig. 4(a), inset),the composed AZO microflakes are regular plates with lengths of about 500nm and thickness of about 30 nm, it can be identified that the crystal grows completely. When the concentration of Zn^{2+}declines to 0.075mol/L in Fig.4(b), the uniformity is less than AZO microflakes in Fig.4(a) and the edge of AZO microflakes becomes rough. The decrease of reactants may lead to incomplete crystal growth.

Fig. 4(c) presents the SEM image of AZO prepared by the concentration of Zn^{2+} (0.05mol/L). It can be clearly seen that AZO has a hexagonal disk shape with a diameter of about 700nm, and the thickness of the disk is measured to be about 100 nm, as shown in the upper right inset. The well-resolved smooth edges and flat hexagonal plane indicate very good crystalline quality of the disk. When the concentration of Zn^{2+} declines to 0.025mol/L, AZO remains hexagonal disk shape in Fig 4(d), while the uniformity become poor and the edge become rough. There are a lot of small particles on the surface of AZO plates. It indicates that the AZO plates grow incompletely because of inadequate AZO particles. Panel of Figure 4(d) reveals that the thickness is less than 50nm atahigh-magnification SEM image. Fig. 4(e) presents the HRTEM image of nanoplates. The 2D lattice fringe spacing is measured to be about 0.28 nm, with an angle of about 60°, corresponding to the $(10\bar{1}0)$ crystal planes of wurtzite ZnO in Fig. 4(f) left. The SAED pattern shown on the right can be indexed as the [0001] zone axis of single-crystalline ZnO with a hexagonal structure.

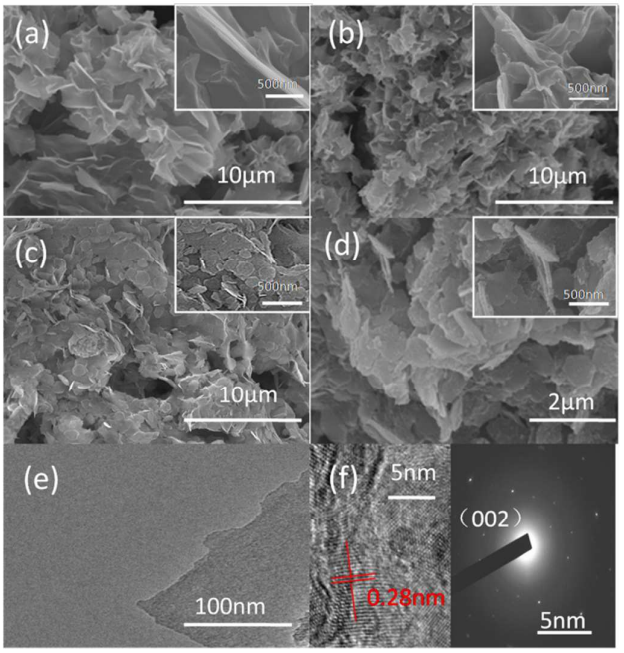

Fig. 4 SEM images of the AZO microstructures prepared at different concentration of $Zn(CH_3COO)_2.2H_2O$ and HMT using pure water as solvent at 120°C: (a) C_{Zn2+} = 0.1mol/L, C_{HMT} =0.2 mol/L; (b) C_{Zn2+} = 0.075mol/L, C_{HMT} =0.15 mol/L; (c) C_{Zn2+} = 0.05mol/L, C_{HMT} =0.1 mol/L; (d) C_{Zn2+} = 0.025mol/L, C_{HMT} = 0.5mol/L. The upper right insets in (a),(b),(c) and (d) are high resolution SEM images of products, respectively (e)TEM image (f)the left is HRTEM image of the hexagonal AZO disk ;the right is thecorresponding SAED pattern.

In this study, we focus on the controllable synthesis of AZO structures with different exposed crystal facets and investigate the effect of the exposed facets on the gas sensing property. Fortunately, we successfully obtained a series of AZO microstructures with different exposed facets by simply adjusting volume ratio of ethanol to water. Fig. 5 displays the SEM images of AZO products corresponding to the volume ratio of ethanol to water from 20:15 to 35:0. In Fig. 5(a) and (b), when the volume of ethanol was 20ml, flower-like AZO structures are formed. It can be seen that the flower-like AZO consists of many disks with diameters of several micrometers. As the volume of ethanol was raised to 35ml, a hexagonal AZO prismoid could be observed with the length of 2.0 μm in Fig. 5(c) and (d), which appear like a dumbbell with both hexagonal prism shape ends about with the length of side of 1μm. The underside of the dumbbell is regular hexagon which is typical structure of hexagonal wurtzite ZnO.

3.3 Growth process

The crystal growth process involves four stages: nucleation, crystal growth, dissolution and re-crystallization. External conditions may have tremendous effects on the morphology

and size of a given crystal by participating in the nucleation and growth, in which many overall factors integrate to dominate the process. The real behavior of crystal growth in crystallites may vary between fractal aggregation in the initial period and the subsequent diffusion process.

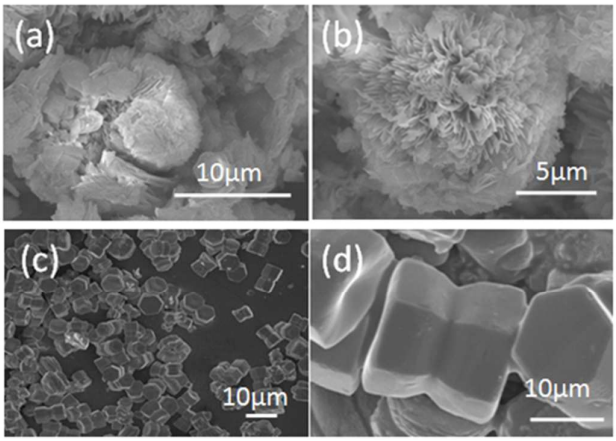

Fig. 5 SEM images of the AZO conversion process by controlling volume ratio of ethanol to water using a concentration ratio of Zn^{2+} to HMT of 1 : 2(C_{Zn2+} = 0.05mol/L) at 120°C: (a)20:15 , (c) 35:0, (b) and (d) are high resolution SEM images of (a) and (c)

The schematic presentation of the possible growth mechanism of the AZO disks is shown in Fig.6. At first, the generation of simonkolleite hexagonal disks was considered to proceed competitively in the solution following the successive chemical reactions:

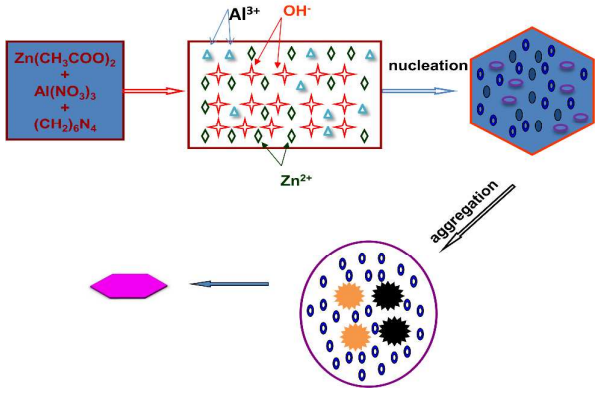

Fig. 6. Schematic representation for the formation of AZO microstructures.

$$C_6H_{12}N_4+10H_2O \rightarrow 6HCHO+4NH_3\cdot H_2O \quad (4)$$
$$NH_3\cdot H_2O \rightarrow NH_4^+ + OH^- \quad (5)$$
$$Zn^{2+}+4OH^- \rightarrow Zn(OH)_4^{2-} \quad (6)$$
$$Al^{3+}+4OH^- \rightarrow Al(OH)_4^- \quad (7)$$

First, $C_6H_{12}N_4$ decomposes into formaldehyde (HCHO) and ammonia(NH_3) as shown in eqn. (4). Ammonia forms ammonium hydroxide in water to produce OH^- anions (eqn. (5)). Secondly, OH^- anion reacts with Zn^{2+} and Al^{3+} to form a homogeneous solution containing $Zn(OH)_4^{2-}$ and $Al(OH)_4^-$ ions that played a key role in the morphology development of the AZO crystallites. (eqn. (6)and (7)) Finally, $Zn(OH)_4^{2-}$ and $Al(OH)_4^-$ after dehydration reduced to Al doped ZnO (AZO).

According to the growth habit of ZnO crystals, the relative rates of the ZnO crystal growth in different directions have been reported[18].Hence, growth units were preferentially supplied for the c-axis direction of every nucleus. During the diffusion, dissolutionand recrystallization processes, stacking together along [0001] direction for the simonkolleite disk is a preferred choice. Because ethanol is a polar solvent, (0001) is a polar plane. The adsorptive rate of ethanol along (0001) becomes bigger. With the addition of the ethanol, the hexagonal disks grew larger and a flower-like microstructure was obtained at volume ratio of ethanol to water of 20:15. Increasing the ethanol volume to 35 ml, more and more disks gathered spontaneously and rapidly to form the dumbbell-like structure with a large c-axis length and a small diameter. To support the growth process, that is illustrated in Fig. 7.

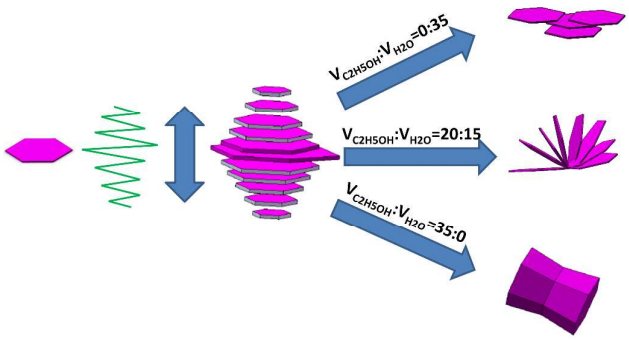

Fig. 7 Illustration of the formation mechanism of various AZO structures

3.4 Gas sensing properties of the sensors

3.4.1 Working temperature

Fig. 8(a) represents the sensitivity characteristics of the AZO powders as a function of operating temperature for 50 ppm of ethanol in air. The response sensitivity varied with the operating temperature. The sensitivity increased between 240 to 332°C, and then decreased in 383°C. The AZO powders show the maximum response at 332°C to 400 ppm of ethanol vapour. The optimum operating temperature of a sensor is 332°C, the mechanism can be explained physical sorption and chemical sorption[19]. At a critical temperature, the chemical reaction and gas transition achieve a balance, and then the gas sensitivity can reach its peak. It's consistent with previous reports[2-3].

3.4.2 Selectivity

Gas sensors for practical applications are required to have very good selectivity to the targeted molecules. Five typical gases (H_2, NO_x, CO, HCHO, CH_3OH, and NH_3) were selected as target gases to investigate the gas response at operating temperature of 332°C, where the concentration of all the tested gases was 50 ppm. The gas sensor based on the AZO microstructures (Fig.8(b)) showed good selectivity to ethanol.

As we know, oxygen adsorption plays an important role in the electrical properties of the AZO sensor. Oxygen ion adsorption removes the conduction electrons and enhances the resistance of AZO. Reactive oxygen species such as O^{2-}, O_2^- and O^- are adsorbed on the AZO surface at elevated temperature, the amounts of such chemisorbed oxygen species depend strongly on temperature. At low temperature about 100-200°C, oxygen molecules in the atmosphere are adsorbed on the surface of AZO and form oxygen ion molecules, while at higher temperatures about of 250-350°C, the oxygen ion molecules are dissociated into oxygen ion atoms with singly or doubly negative electric charges by attracting an electron from the conduction band of AZO[20].

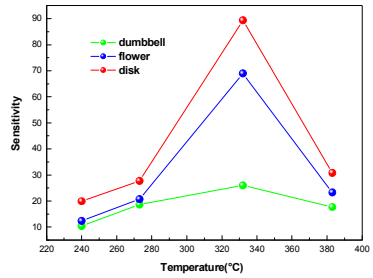

(a)

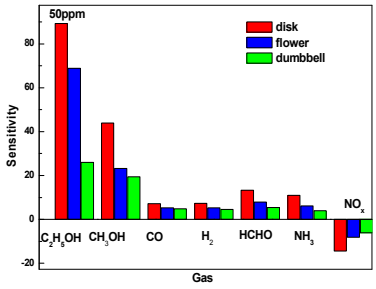

(b)

Fig. 8 (a) Relationship between the response and the working temperature of the sensors to 50 ppm ethanol vapor. (b) Gas response of thesensors to 50 ppm various gases at the optimum working temperature of 332°C

Here, the ethanol-sensing mechanism of the AZO sensor is originated based on the semiconductor oxides, due to the oxidation or reduction of the semiconductor oxide, according to the dissolved O_2 in the surface air of the neighboring atmosphere, described as shown in Eqn. (8) and (9):

$$e^- (AZO) + O_2 \rightarrow O_2^- \quad (8)$$

$$e^- (AZO) + O_2^- \rightarrow 2O^- \quad (9)$$

These reactions are attained in the bulk system, adjacent atmosphere owing to the small carrier concentration, which improved the resistance. The ethanol sensitivity toward AZO could be attributed to the high oxygen deficiency, which increases the oxygen adsorption. The larger the quantity of oxygen adsorbed on the sensor surface, the larger would be the oxidizing potentiality and the faster would be the oxidation of ethanol. Ethanol reacts with the adsorbed oxygen on the exterior/interior of the layer, it oxidized to CO_2 and H_2O, accompanied by the release of six electrons in the conduction band, which could be expressed through the following reaction:

$$C_2H_5OH + 6O^- (ads) \rightarrow 2CO_2 + 3H_2O + 6e^- (10)$$

From the above typical reactive formulas, it can be found that, to the same concentration of target gases, ethanol released more electrons than other gases. This may be the reason why AZO sensor has a good ethanol sensing properties.

3.4.3 Response-recovery characteristic

The response-recovery behavior is an important characteristic for evaluating the property of gas sensors[21]. Fig. 9(a) exhibits the response and recovery curves of all sensors upon exposure to 5, 10, 30, 50, 100, 200 and 500 ppm ethanol at the optimum operating temperature. Fig.9(b) shows the relationship between response and ethanol concentration. It can be clearly seen that the response of the sensors toward ethanol reduces dramatically, associated with the evolution of the microstructures from hexagonal disk to dumbbell. For example, their responses to 50 ppm ethanol are 89.35(disk), 68.93(flower) and 26.01(dumbbell), respectively. The response of the AZO flower-based gas sensor to ethanol is more than 3 times higher than that of the dumbbell-based sensor. Moreover, even though the ethanol concentration is down to 5 ppm, it can still be detected by the sensor based on the AZO disks with a response of 20.43, while the responses of the other sensors are no more than 5. Fig. 9(d) displays the enlarged response-recovery curves of the sensors toward 50 ppm ethanol. It can be found that the response time of all sensors is about 50 s, while the recovery time increases from 10 s to 13 s and 30 s, accordingly. The reason is probably that the flower-like AZO is in high-energy metastable state, chemisorption is easy while the desorption of chemisorbed gas molecules is difficult. In the meantime, the bigger the value of the response is, the more difficult the recovery is.

Fig. 9(c) shows the correlation between variation in sensitivity of the AZO sensor and ethanol concentrations ranging from 5 to 500 ppm at 332°C. At lower concentration, it can be observed that for all the tested gases, there is a linear relationship between log (S - 1) and log (C), which is in good agreement with the theory of power laws for semiconductor sensors [21,22]. The b value (0.50083) of AZO microdisk sensor is very close to 0.5, indicating that the adsorbed surface oxygen species is O_2^- , in accordance with the report that the dominated oxygen species on AZO surface is O_2^- above 300°C.The same is as the other two microstructures of AZO. At higher concentration, the surface coverage tends to saturate and hence leads to the saturation response. There would be gas molecules on the sensor surface at the higher gas concentrations resulting in saturation in gas response. The result indicates that AZO sensors are a good new gas sensing material for detecting ethanol. By comparison, table 3 lists the sensing performance of our AZO sensors against previously reported AZO by different preparation method.

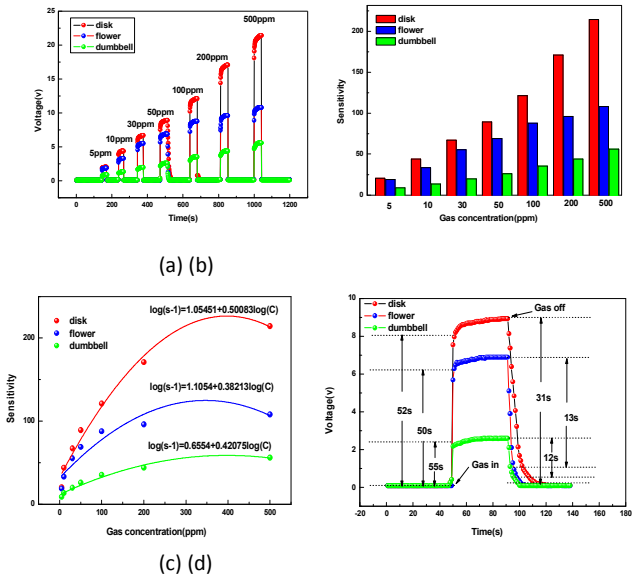

Fig. 9 (a) Dynamic sensing characteristics of the sensors towards ethanol vapor of various concentrations. (b) The corresponding response of the sensors. (c) Response of the sensors (S) vs. ethanol concentrations (C). (d) Response-recovery curve of the sensors to 50 ppm ethanol vapor.

Table 3 Research of the Sensing Performances of Various AZO Sensors Toward ethanol

Preparation method	Ethanolconcn (ppm)	Operatingtemp (°C)	Sensitivity(S = Ra/Rg)	Ref
Grinding in an agate mortar	1000	290	~108	[3]
Thermal evaporation	500	300	99.9	[7]
Hydrothermal	500	332	~214	In this paper

3.4.4 Gas sensing mechanism

It's well-known that most metal oxide semiconductor gas sensors are based on the conductivity. The sensing process mainly involves the gas adsorption, charge transfer, and gas desorption[23], as represented by Fig. 10. There are a number of donor defects in the ZnO crystal structure, and the radius of Al^{3+} is larger than that of Zn^{2+}, therefore it's easy to form effective Al doping in ZnO crystals. The electron produced by the defects of O or Zn in ZnO without Al, while after Al doping, the lattice position of Zn^{2+} is replaced by Al^{3+}, which caused an extra electron and an oxygen vacancy, the amount of the current carrier is bigger. It amounts to potential energy barrier of electronic transition fell, the conductivity strengthened.

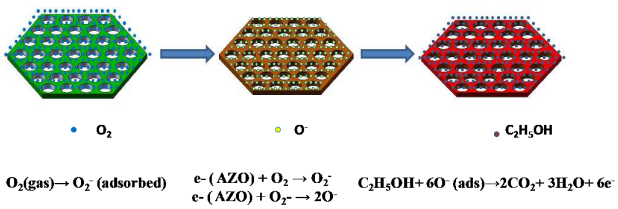

Fig. 10 Sketch of the possible ethanol sensing process on the hexagonal AZO disk-based sensor

On the other side, it has been well known that the gas sensitivity of AZO is strongly dependent on its morphology. The BET surface area of AZO, micodisks, microflowers and microdumbbells were 18.5,16.9 and 12.5 $m^2 g^{-1}$. For AZO with homogeneous disk-like morphology, microdisks provide larger contacting surface area with more reactive sites for electrons, oxygenand target gas, and the voids and interspaces existing among microdisks facilitate gas adsorption and desorption.

It is widely known that the exposed (0001) facets of ZnO crystal structure can provide more active sites for oxygen adsorption and subsequent reaction with the detected gas than other polar facets and thus increase the gas sensing response[24,25]. Moreover, for hexagonal ZnO, Zn atoms on the surface are usually coordinatively unsaturated[26], and more dangling bonds exist on the (0001) surface than on the $(10\bar{1}0)$ surface. It can be inferred that, because of the high activity, the adsorption of ionized oxygen species is more likely to occur on the (0001) plane of hexagonal ZnO rather than on other planes. For this reason, there will be more oxygen species on the (0001) polar planes than on $(10\bar{1}0)$ polar planes, and thus the gas sensor based on hexagonal AZO disks predominantly exposed with (0001) facet shows better gas-sensing properties than other sensors based on the hexagonal AZO flower and dumbbell with more exposed $(10\bar{1}0)$ facets.

4.Conclusions

In this paper, AZO disks, flowers and dumbbells are successfully obtained through a simple hydrothermal method from a hexagonal simonkolleite disk precursor by adjusting the volume of the solvent. The precursor disks are suggested to stack with each other along the [0001] direction. With the evolution of the structures, less (0001) crystal planes are exposed on the total surface. The gas sensing properties of these structures are degraded dramatically as well. This superior gas sensing performance strongly depends on the exposed crystal plane with the polar facets of (0001). The results demonstrate that it is a significant and promising method to control the exposed facet of an AZO crystal structure for the fabrication of a high performance gas sensor.

5. Acknowledgments

This work was financially supported by Provincial Science and Technology Agency(No. 12533042) and Provincial Academician Guiding Project(No.201310234005).

References

1 Doty, R. L.,Cometto-Muniz, J. E.,Jalowayski, A. A., Dalton, P., Kendal-Reed, M. and Hodgson, M, Crit. Rev. Toxicol, 2004,34,85.
2 P.P. Sahay and R.K. Nath, Sens. Actuators B, 2008,134, 654.
3 Zunxian Yang and Yun Huang, Sens. Actuators B,2009, 140 ,549.
4 Satish S. Badadheand I.S. Mulla, Sens. Actuators B, 2011,156, 943.

5 M.H. Huang, S.Ma H. Feiek and H.Q. Yan,Nanolasers Science, 2001,292,1897.
6 S.C. Navale and V. Ravi, Sensors and Actuators B, 2007,126,382.
7 L.M. Li, Z.F. Du andT.H.Wang, Sensors and Actuators B 2010,147,165.
8 Yue Hou and Amir M, Soleimanpour, Sensors and Actuators B,2013, 177,761.
9 Vaishampayan, Mukta V., Deshmukh, Rupali G. andMulla, I. S, Sens. Actuators B, 2008,131, 665.
10 Deliang Chen andLianfang Ge, Sens. Actuators B 2014,205,391.
11 Korotcenkov, G,MATERIALS SCIENCE & ENGINEERING R-REPORTS, 2008,61,1.
12 Ogheneyunume Obi and Ziyao Zhou, J Mater Sci: Mater Electron,2013,24 ,2058.
13 Wei-Jen Chen and Jen-Kai Wu,Nanoscale Research Letters 2013,8,313.
14 Seong-Ho Baekand Bum-Young Noh, Nanoscale Research Letters 2012,7,29.
15 Xi Fan and Guojia Fang, Nanoscale Research Letters 2011,6,546.
16 EsinBurunkaya and Nadir Kiraz, J Sol-Gel SciTechnol,2010,55 ,171.
17 Li Zan, Qin Wei, Zhao Wenjie and Wu Xiaohong, Functional Materials Letters,2014, 7 ,1450037.
18 A. Smith, R. Rodriguez-Clemente, Thin Solid Films,1999,345 , 192.
19 S.R. Morrison, the Chemical Physics of Surfaces 2nd, Plenum Press, New York,1999, p. 251.
20 NiyomHongsithandEkasiddhWongrat, Sens. Actuators B , 2010,144, 67.
21 Lexi Zhang andJianghong Zhao, Sens. Actuators B,2011,158 ,1440.
22 Yuan Zhang andJiaqiang Xu, J. Phys. Chem. C, 2009,113,3430.
23 Z. Gergintschew, H. Förster, J. Kostiza and D. Schipanski, Sens. Actuators B,1995,26, 170.
24 G. R. Li, T. Hu, G. L. Pan, T. Y. Yan, X. P. Gao and H. Y. Zhu, J. Phys. Chem. C,2008,112,11859.
25 O. Dulub, U. Diebold and G. Kresse, Phys. Rev. Lett., 2003,90, 16102.
26 C. Wöll, T.Prog. Surf. Sci., 2007,82,55.

